Overview of liquid metal PFC R&D at the University of Illinois Urbana-Champaign

D. Andruczyk[1], R. Rizkallah[1], D. O'Dea[1], A. Shone[1], S. Smith[1], B. Kamiyama[1], R. Maingi[2], C. E. Kessel[3], S. Smolentsev[3,4], T. W. Morgan[5] and F. Romano[5]

[1]University of Illinois Urbana-Champaign (UIUC), Urbana IL, USA
[2]Princeton Plasma Physics Laboratory (PPPL), Princeton NJ, USA
[3]Oak Ridge National Laboratory (ORNL), Oak Ridge TN, USA
[4]University of California Los Angeles (UCLA), Los Angeles CA, USA
[5]Dutch Institute for Fundamental Energy Research (DIFFER), Eindhoven, The Netherlands

Corresponding email: andruczy@illinois.edu

Abstract

The design and implementation of future flowing liquid lithium PFCs (LLPFC) will be dependent on several factors. Of course, one of the most important is the need to be able to deal with high heat fluxes incident on the surface of the LLPFC but there are also several other important LM behaviors that have been identified for their critical impact on the feasibility of a LLPFC. One of these is the ability to constantly wet 100% of the PFC area and the best way to achieve that. Another key point is knowing and understanding the erosion and corrosion of the surfaces subject to a flowing liquid lithium system and the ability for hydrogen and helium uptake by the system. The Center for Plasma Material Interactions (CPMI) was tasked at looking at these various issues. The MEME device was used to investigate wetting and erosion effects and design a suitable distribution and collection system with a liquid lithium loop. Vapor shielding effects of lithium on the surface were also modeled and studied. A model coupling CRANE, an open source global reaction network solver, and Zapdos, a plasma transport solver, is being developed to better understand the dynamics of the vapor cloud. Experiments on Magnum-PSI at DIFFER have been carried out to study the vapor shielding effect and obtain experimental benchmarks to verify the model. Also, initial experiments using HIDRA have been performed to understand the pumping effects of lithium on helium. Experiments with a drop of liquid lithium (~100 mg) into a helium plasma have showed the ability for lithium to take out the cold recycling helium gas as well as hydrogen and oxygen impurity gases. The improvement in plasma performance was significant and further understanding of this effect will have impacts on how future LLPFC will be designed. Further investigation into the exact mechanism for helium pumping by lithium needs to be performed in the future. This paper presents a summary of the results obtained at CPMI.

I. Background

The ability for plasma facing components (PFCs) to survive the harsh environments of an operating fusion reactor over a long time is one of the main detriments to an operating commercial device. This makes the development of PFC of the utmost importance. Currently solids materials such as tungsten are the leading candidate but have several issues such as tritium retention [1,2], surface degradation [3] and fuzz and bubble formation [4,5]. Flowing liquid metals such as lithium offer at least a solution to protecting the surface of the underlying substrate [6]. Thus, a fusion nuclear science facility (FNSF) has been proposed as an intermediate step to finally figuring out the materials issues for a fusion reactor [7]. Liquid metals pose a potential solution in particular lithium. However, lithium has its own engineering issues that need to be addressed. A study of liquid metals for FNSF was done by Kessel et al., [1,7] and identified several

challenges that implementation of a liquid metal PFC system would have [8]. However, the many benefits that come with using lithium as a liquid metal PFC potentially outweigh any detraction [9-13].

To this end the U.S. department of energy has implemented a domestic liquid metal PFC development program with the direct aim of eventually designing a flowing liquid metal divertor for an FNFS or compact pilot plant (CPP) [14]. The aim of the program is to evaluate liquid metal (LM) PFC concepts through engineering design calculations, modeling and experiments [14]. Lithium was selected as the LM of choice since it's the most well studied of the PFC candidates. Three institutions were chosen to lead the program: the Princeton Plasma Physics Laboratory (PPPL), the Oak Ridge National Laboratory (ORNL) and the University of Illinois at Urbana-Champaign (UIUC).

The goals of the UIUC part of the LMPFC program consist in performing single effect experiments that will further the engineering understanding of liquid lithium systems and in identifying potential issues and developing solutions. Three main tasks can be identified:

1. *Liquid Lithium Loop and wetting of surfaces* – This is to develop a full flowing liquid lithium loop system with an integrated loading system, LM pumps and flow velocity measurements. An important aspect to this is the need to have an effective distributor design that will ensure an even distribution of lithium down a surface as well as ensure full wetting of a surface when flowing lithium. The full wetting of surfaces has been problematic in past experiments [15] and will need to be resolved for future devices.
2. *Lithium vapor shielding* – The effect of lithium vapor shielding (LVS) is a phenomenon that has been observed and identified recently [16,17]. The effect of impurities such as helium and neon in the plasma is an unknown on the effect it will have on the ability of the LVS to dissipate incoming heat flux from the plasma. Helium will be a natural impurity derived from the $D + T \rightarrow He + n$ reaction and neon is currently one of the candidates neutral seeding gases for plasma detachment in the divertor region. We aim to develop a better understanding of the effect through experiments on Magnum-PSI and through modeling using plasma transport model and plasma chemistry codes such as Zapdos-CRANE [18].
3. *Hydrogen and helium retention by lithium* – One of the main arguments against lithium is that it will react with and retain tritium, but also will not be able to retain and pump helium. Helium pumping is an issue in fusion as turbo pumps take a long time to pump helium effectively and cryogenic pumps do not pump helium. It is important to know and understand the rate at which hydrogenic species will be captured by lithium, the rate at which they can be removed [8] and whether lithium is able to pump, retain and remove helium from the plasma [19].

This paper will summarize some of the results from the initial single effect experiments that have been undertaken at UIUC as part of the domestic LM PFC (LMPFC) program.

II. Distribution and Wetting

Operation of a flowing liquid lithium system will require several engineering technologies to come together effectively. The first is a flowing liquid lithium loop, a closed system which would enable lithium circulation with flow control. The second is an effective means to ensure distribution of the lithium over a surface to achieve full coverage. This is tightly connected to surface wetting and is known to change for different metals and different temperatures [20]. Last is an effective way to load lithium into the loop without air leakage which can contaminate the lithium.

Previously an international collaboration between several US institutions and the EAST team [15] performed experiments on EAST designed to tackle some of the questions connected to flowing lithium

technologies and had several positive outcomes. The experiments successfully flowed liquid lithium over surfaces with different geometries and demonstrated improved plasma performance. However, surface wetting was not total and there is still a long way to go before having a fully integrated and flowing system. The tested FLiLi [15,21-23] and LiMIT [24,25] plates were connected to an internal reservoir and electromagnetic (EM) pump system, moving the lithium through a distributor, down the plate surface and around, but not out of the machine. Out of this previous program the Mock-up Entry module for EAST (MEME) was designed and built for UIUC to further research and develop such liquid metal systems. It is based on the Material and Plasma Evaluation System (MAPES) system [26,27] that allows LM systems to enter the EAST vessel without breaking vacuum.

II.A. Description of the Mock-up Entry Module for EAST (MEME)

The motivation of obtaining MEME was to have a system where LM systems could be developed with an interface with EAST. The system is a cube-box that with dimensions of, *1.0 m × 1.0 m × 1.0 m*, with a total volume of V_{MEME} = 1.0 m³. This is in fact much larger than the LiPES system installed on EAST, which is, *0.65 m × 0.65 m × 0.65 m*, with a total volume of V_{LiPES} = 0.275 m³. There is a 1 m stroke length transfer arm that LM systems can be mounted on. The transfer arm allows access for power, cooling and thermocouples to any LM system. A turbo-molecular pump of 1000 L/s rate evacuates MEME down to base pressures of P_o ~1.2×10⁻⁵ Pa (9×10⁻⁸ torr). A Pfeiffer Full Range gauge measures the pressure. MEME has 25 ports of varying sizes which gives a vast choice for choosing viewing ports and mounting diagnostics. In addition to the previously mentioned full range gauge and RGA, color and infrared cameras are installed to monitor ongoing experiments. There is an internal attachment on the transfer arm that allows for some rotation of any mounted LM surface, enabling the study of flowing systems under different angles. Figure 1 shows a photo of MEME in its current set up with an image of the rotation mechanism superimposed on a CAD of MEME.
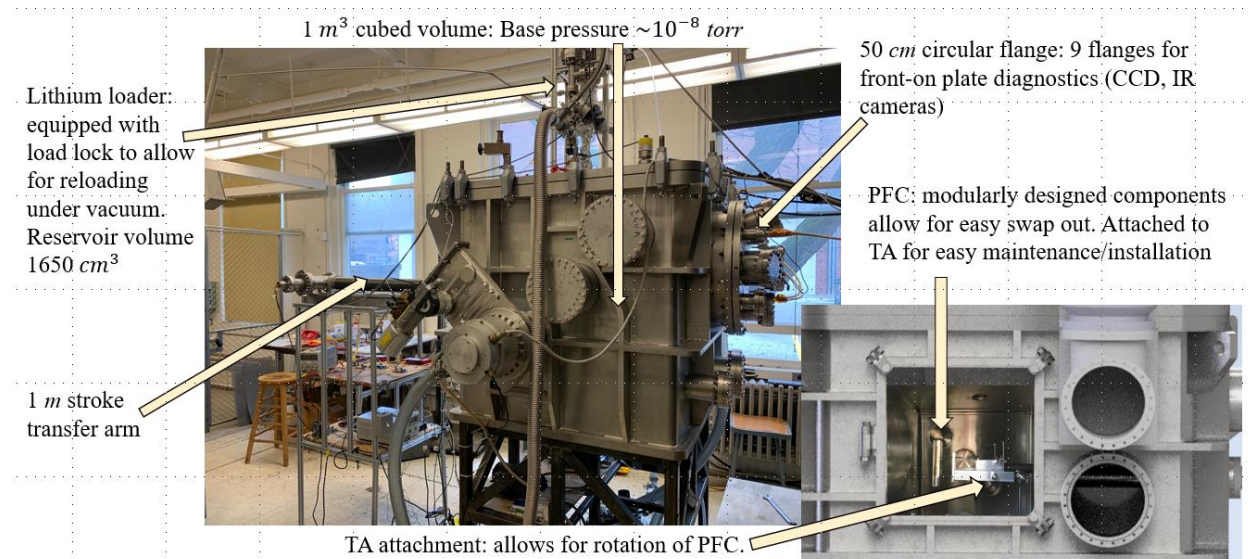
Figure 1: Mock-up Entry Module for EAST (MEME). The system is based on the LiPES system used on EAST and is designed to develop plug-and-play LM systems for EAST. Currently it is being used to develop LM loops and wetting experiments for the LMPFC program.

Though MEME was designed with EAST in mind, it serves as a perfect tool for the domestic liquid metal PFC program and the testing and development of liquid metal loops as well as surface wetting experiments. Its large volume facilitates experiments design and mounting of the various necessary systems, such as the

ones needed in developing a fully operational lithium loop system connected to a PFC plate of a desired geometry.

As part of the LMPFC program, the flowing LM development was divided into three milestones, the first of which is the development of a flowing lithium loop along with liquid metal pumps and flow sensors. The second is develop a lithium loading method in a way such that the lithium will not be tarnished due to undesired exposure to air. The last milestone is to achieve full surface wetting for the lithium to evenly coat the surface.

II.B. Flowing Lithium Loop Experiments

Figure 2 shows the flowing liquid lithium loop installed in MEME. The aim of this loop is to deliver lithium to the distributor and surface. The internal reservoir (red) is filled with lithium from an external loading system. The lithium is heated to 270 °C. At the moment this seems to be the limit of the heating system. Because of that, the pipes in the loop may not be wetting completely, since the wetting temperature for stainless steel is 320 °C [20]. The lithium melts and flows into the pipe connected to the first LM pump (purple). The LM pump is a standard electromagnetic (EM) pump with a current passing through the lithium and a perpendicular magnetic field. The resulting $J \times B$ force moves the liquid lithium up a vertical section and into a second liquid metal pump (pink). This is also an EM pump that helps to flow the lithium to the distributor. The current required for EM pump 1 is $I_1 = 129$ A and for EM pump 2 is $I_2 = 100$ A.

(a)   **(b)**
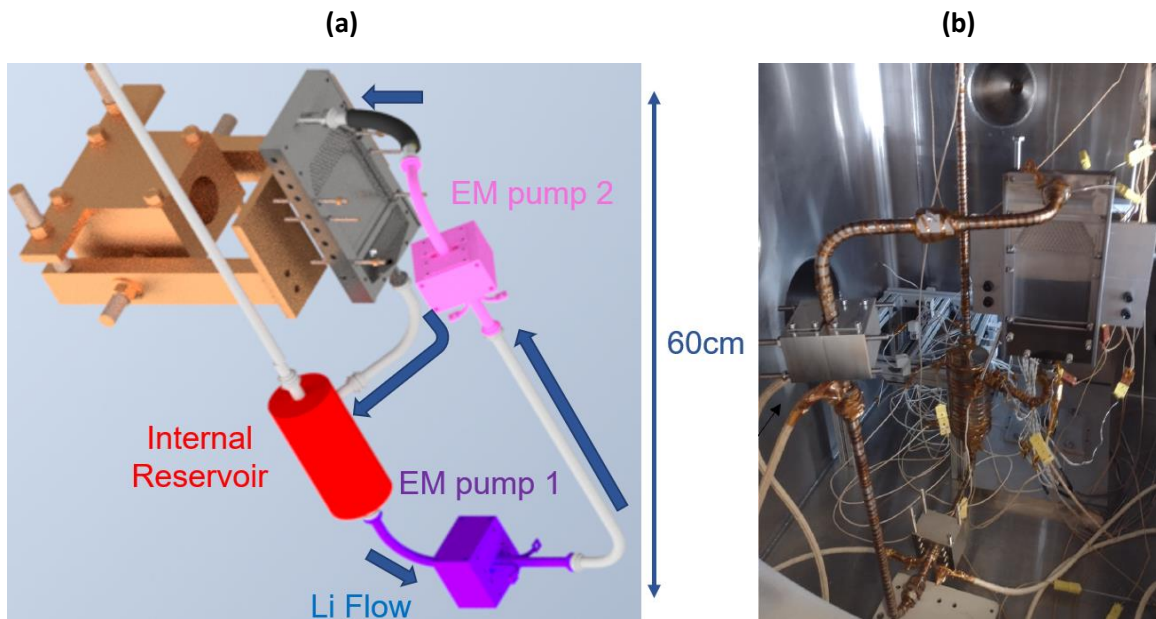
Figure 2: (a) CAD drawing of the internal flowing liquid Li loop that is installed and being tested in MEME for the program. The internal reservoir (red) has lithium loaded into it via and external loading system. Once the lithium melts and the system reaches 270 °C the lithium flows into the first EM LM pump (purple) this pumps the Li up to the second EM LM pump (pink) and to the distributor and PFC plate (gray) system for wetting studies. This is then collected and flows back to the internal reservoir completing the whole loop. The system has been continuously run for several 10's of minutes at a time. (b) Actual photo of the internal loop inside MEME.

The distributor is based on the posts LiMIT design [28] to try and help distribute the lithium evenly across the surface of the attached plate. As the lithium flows down the plate surface, it is collected in a collector and flown back into the loop reservoir. This completes the loop which can continuously flow the lithium around. The whole system is mounted to the transfer arm and can be tilted to about 13° under the current setup. This is only a restriction of the current design and future redesign of the system will allow for larger angles to be explored. There are seven thermocouples (TC) that are attached to the loop and a further six TCs on the plate itself to monitor the temperature of the different sections of the system. A total amount of 300 g of lithium is loaded into the loop reservoir before the experimental runs. Figure 2(a) shows a CAD of the loop system and figure 2(b) is a photo of the loop inside the MEME chamber.
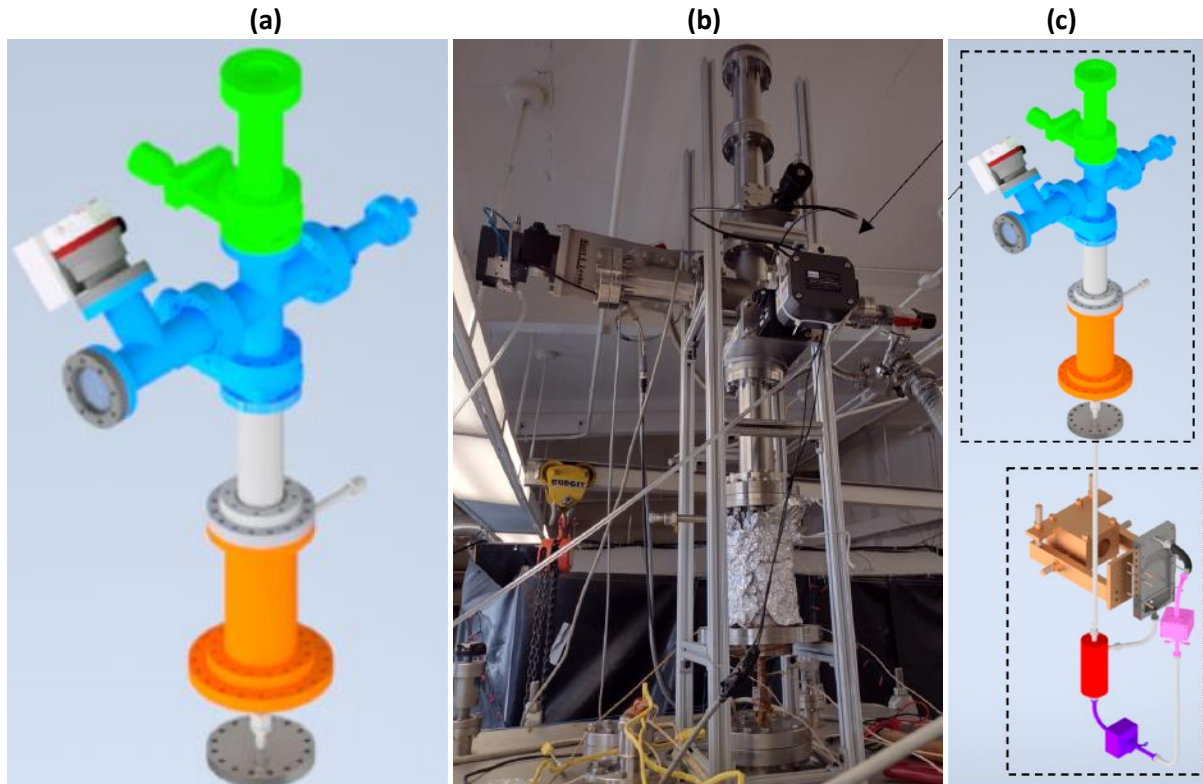

Figure 3: CAD of the lithium loading system that is used to load lithium into the lithium Loop on MEME. A "suitcase" (green) has the lithium loaded in a glovebox filled with argon. This then attaches to an evacuation system (blue) where the argon is pumped out and the lithium is pumped to low pressures to minimize the amount of tarnishing of the lithium. This is then dropped into a pre-melting reservoir (orange) where the lithium is melted and then flows through a pipe into the internal reservoir of the loop. (b) Photo of the lithium loading system on MEME. (c) CAD showing the Li loading system connected to the Li loop system.

The lithium is loaded into the loop via a lithium loading system. A CAD of this is shown in figure 3(a) and a photo of it as mounted on the top of MEME is shown in figure 3(b). A suitcase (green) is loaded with lithium inside an Argon filled glovebox. Argon, which also fills the suitcase, is an inert gas and minimizes the amount of tarnishing of the lithium. The suitcase is a Con-flat flange with one end sealed and the other connected to a gate valve. Once loading is complete, it is then mounted onto the loading station (blue) and pumped out. The lithium is then dropped into a melting chamber (orange) where it is melted. Once sufficiently hot, the lithium flows down into the internal reservoir of the loop. A CAD of how the loading system and lithium loop link together is shown in figure 3(c).

II.C. Initial Distributor Tests and Flow Velocity

For the initial lithium distribution tests, a color camera was used to observe the flowing lithium over the studied plate. The distributor which has a dedicated cover plate had initially its posts exposed as seen in figure 4(a). However only droplets of lithium were formed as the lithium came out of the loop and unto the distributor. Such droplets can also be seen in figure 4(a). These droplets most often would skip the distributor posts surface and flat plate altogether and go straight down to the collector. Nonetheless, when a droplet would hit the stainless-steel plate at 320 ℃, it did seem to wet the plate surface. It was clear that the distributor cover plate needed to be installed to force the lithium through the distributor posts and improve distribution before reaching the plate. This should also improve lithium wetting at the plate level. With the distributor cover installed, a stream of lithium formed and flowed down the plate. The lithium flow is still only a stream and did not fully spread unto the plate, but it did clearly wet the region along that stream. A 2 mm gap between the distributor cover plate and the top of the posts could be at least partially blamed for the suboptimal lithium distribution as the lithium was able to flow down the distributor cover and then onto the plate. Design modifications along different distributor geometries are being investigated to improve on these results. The loop operation in these initial distribution experiments was for over 30 minutes, and this has been repeated consistently multiple times. Flow of the lithium in the loop was confirmed via the multiple installed thermocouples as the lithium went past temperature changes.

(a)   **(b)**
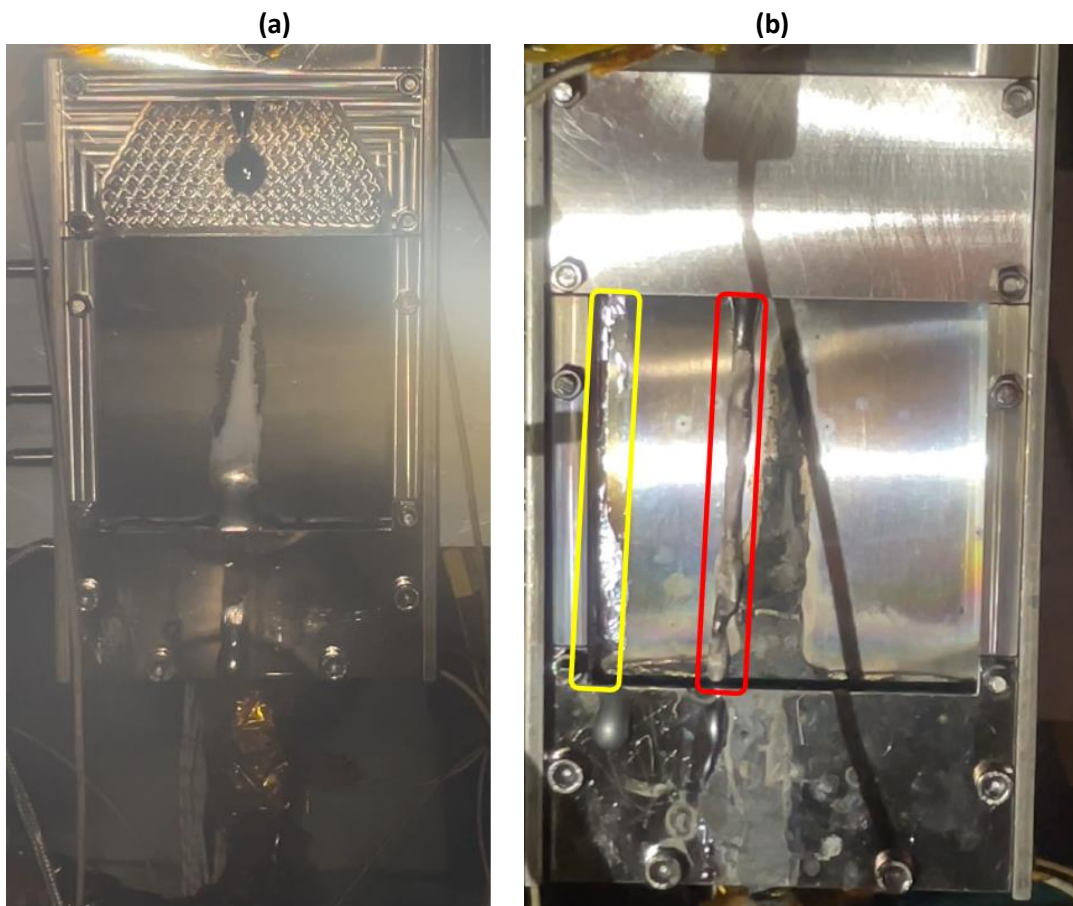
Figure 4: (a) Initial loop and distributor tests in MEME show that when Li gets on the stainless-steel plate there is wetting. The distributor posts are clearly seen. (b) The cover plate is now installed, and a clear stream of flowing liquid Li is flowing down the plate.

In figure 4(b) the distributor is mounted with its cover plate and two lithium streams can be seen. When first switched on (for the runs with the distributor cover), the lithium started flowing down the left side, which is highlighted in the yellow rectangle. This was most probably due to a blockage that was there from some previous runs. As the current in the second EM pump was increased the blockage was cleared and the lithium stream moved to the plate center region, highlighted in the red rectangle.

The flow characteristics of the lithium stream change as the current of the second EM pump changes. In figure 5(a), there are several frames showing how the flow evolves with varying pump currents, going up to 100 A. The flow starts with single drop of lithium and then forms into a continuous flow but presents some oscillations and instabilities. Eventually as the maximum current in the pump is reached a laminar type of flow is reached and the flow becomes even down the plate. The plate area around the lithium stream is wetted by the lithium which follows the wetted path. Flow meters to measure the flow velocity are still being developed, however an estimate of the flow can be obtained from tracking features present in the flow down the plate. Figure 5(b) shows more frames where a feature, a bulge in the flow, moves down the plate. The estimates of this are about $v_{flow} = 1$ m/s.
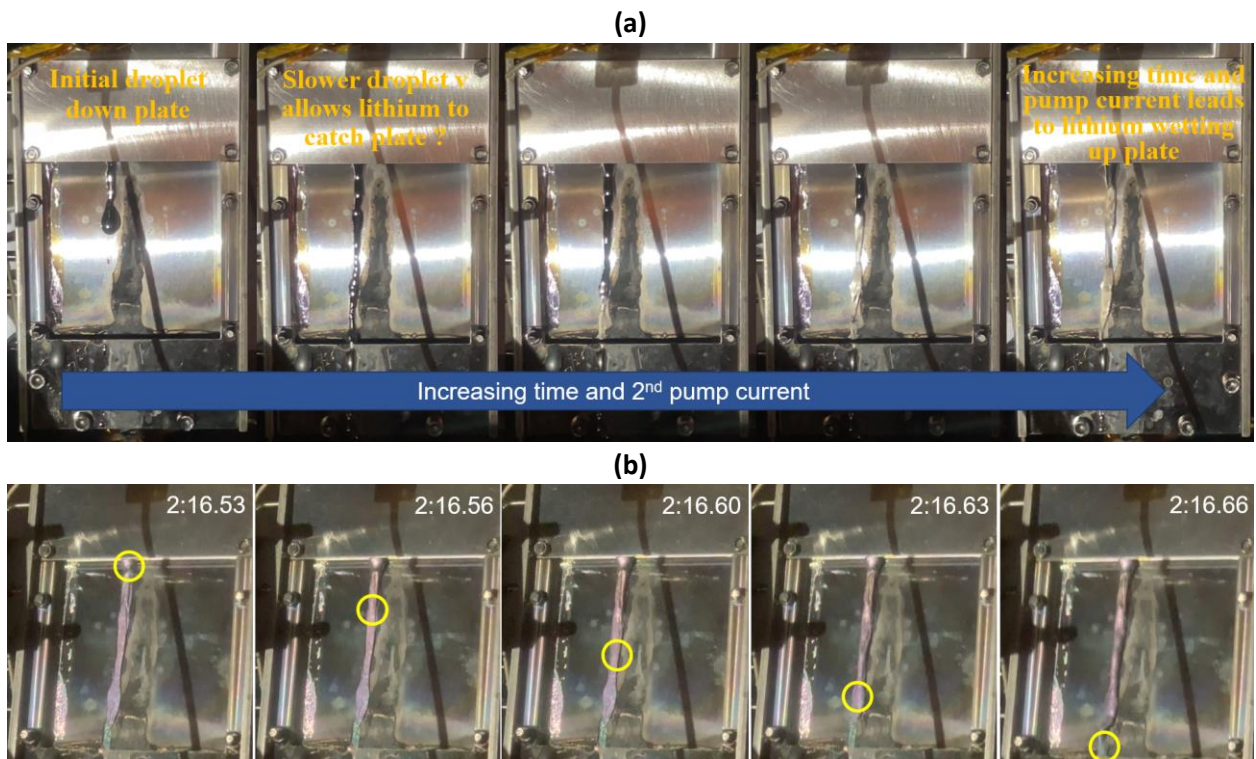
Figure 5: (a) changes in the flow of the lithium with increasing EM pump current. Going from drops to an unstable flow to a stable laminar flow. (b) the flow velocity is estimates by looking at a bulge feature that travels down the flow and is measured to be I m/s.

III. Lithium Vapor Shielding

A phenomenon that has been observed with lithium in recent years is that of lithium vapor shielding (LVS). When subject to an incident heat flux, the lithium evaporates and creates a lithium vapor cloud above the surface. This cloud is suspected to radiate a portion of the upstream heat fluxes away from the lithium surface, extending its operational window. The first published characterization of the effect was performed by van Eden et al. [16] in tin and Rindt et al. in lithium [17,29] on Magnum-PSI [30]. When the vapor

shielding regime is achieved a locking temperature of the liquid surface is attained. That is, the liquid surface maintains this temperature even with increasing heat fluxes. This is a strong suggestion that the formed vapor cloud in between the liquid surface and upstream plasma radiates considerable amount of
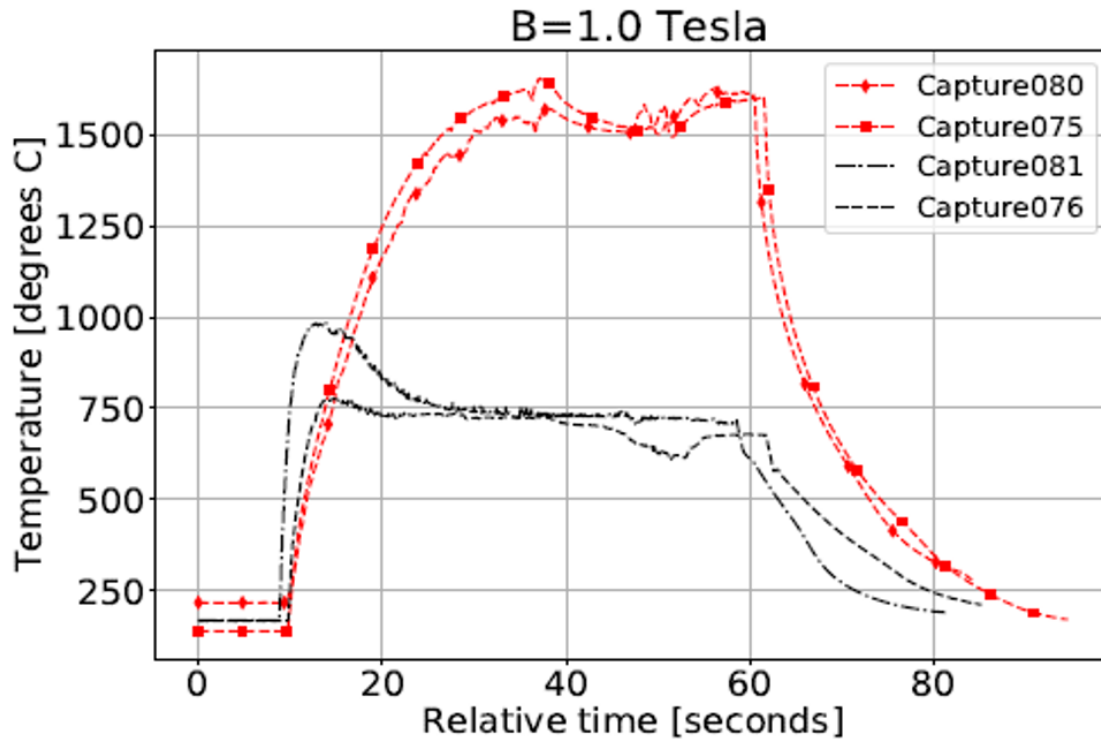

Figure 6: Example of the lithium vapor shielding. 15 - 20 MWm^{-2} heat flux discharges without lithium (red) and with lithium (black) where the locking temperature is clearly observed.
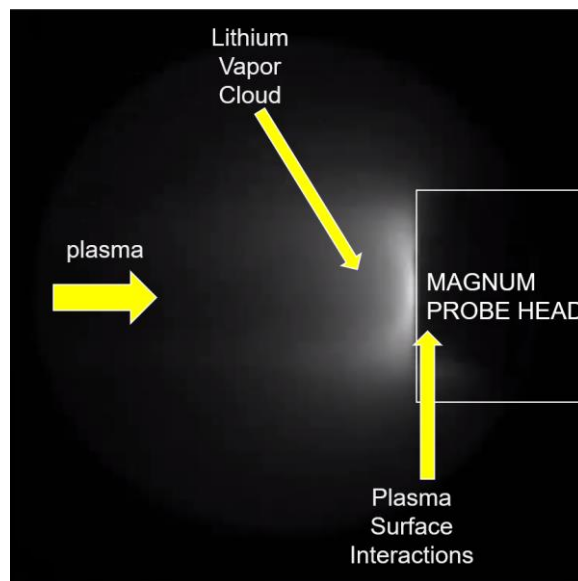

Figure 7: Image showing where the MAGNUM-PSI probe head is with plasma surface interactions and where the lithium vapor cloud occurs. The plasma is coming in from left to right.

power away from the surface, allowing it to maintain this locking temperature. This typically is seen to be between 750 °C – 800 °C for lithium. There is a minimum heat flux required to reach the conditions where the LVS is observed, as too low of a heat flux does not allow for a dense enough lithium cloud to form. Experiments carried out on Magnum-PSI suggest that LVS starts to be significant with around $q = 6$ MW.m^{-2}, with heat fluxes up to $q = 20$ MW.m^{-2} observed to be handled by LVS as seen in figure 6. The surface used to perform these Magnum-PSI experiments was a capillary pore structure (CPS) [31,32] that is 3D printed in tungsten. Figure 6 shows the temperature evolution of both lithium targets and solid molybdenum reference targets with plasma powers of 15 MW.m^{-2} and 20 MW.m^{-2}. The red lines correspond to the solid reference target while the black lines are for the lithium ones. The locking temperature appears to be around 750 °C. By the time these shots were made, the transmission of the windows was very low, and determining its exact value along with the exact surface emissivity of lithium is not possible. Still, the locking temperature phenomenon is clearly seen, sitting within its expected range.

These measurements were done using hydrogen as the fueling gas, however it is critical to know how the LVS effect will behave with certain impurities present. Helium will be generated via the fusion reaction

$$D + T \rightarrow He(3.5\ MeV) + n(14.1\ MeV),$$

and will need to be removed. This will be done via the divertor and if a flowing liquid lithium system with LVS is operating, the helium could have an effect on operation. The other impurity of interest is that of neon, which is potential candidate gas for plasma detachment. Thus, a campaign of LVS with helium and neon impurity seeding in Magnum-PSI was undertaken as part of the LMPFC program. Since a divertor is to be designed, understanding how LVS will behave with these impurities is crucial.

Furthermore, a model is being developed to predict and provide some of the input numbers for the LVS effect to combine this into the SOLPS-ITER calculations being developed as part of the LMPFC program. The goal here is to do calculations to see the plasma response, via SOLPS-ITER, with injected neon and lithium with a three-plate FNSF geometry [33].

III.A. DIFFER Experiments

Figure 7 shows an image of the probe head on Magnum-PSI. The heat flux is measured using steady-state calorimetry. In figure 8 colorimetry data shows the vapor shielding effect on the Magnum-PSI targets under three different power settings. Each of these power settings ranging between 4 MW.m^{-2}, 6 MW.m^{-2} and 8 MW.m^{-2} were used with both a lithium and molybdenum reference target, with a pure hydrogen plasma and with the addition of helium and neon species. The control shot using a non-lithiated molybdenum reference target under a pure hydrogen plasma is in blue. This measured the absolute heat flux generated by the plasma and hitting the surface. Next a pure hydrogen plasma with the same source current and magnetic field setting was generated against a lithium surface shown in orange. Third the lithium target is subject to the hydrogen plasma with neon seeding, shown in green. This is about 1% of the density of neon. Finally, the lithium target was subject to a hydrogen plasma with helium seeding, shown in red.

For the 4 MW.m^{-2} shots there is not much difference between the different plasmas being used and between the lithium and reference targets in the calorimetry data. As seen in figure 8, at this power setting, all 4 curves lay around the same level. However, at the two higher heat fluxes (6 and 8 MW.m^{-2}) the measured heat flux to the surface locks around $4.5 - 5$ MW.m^{-2} for the lithium targets, whereas it increases for the solid reference target. The cloud is therefore dissipating about 1.5 MW.m^{-2} at the intermediate power setting and about 3 MW.m^{-2} at the highest power setting. Figure 8 also shows that below a certain incident heat flux level, the vapor shielding effect is not observed. It is clear that there needs to be a minimum heat flux to the surface to start to evaporate lithium sufficiently for the vapor cloud to properly form and be dense

enough to effectively radiate power away. Figure 8 also shows no effect of adding helium or neon to the system. At the low temperatures of Magnum-PSI, the ionization fraction of these species is so low that they do not affect the system much. Investigating neutral vapor shielding in a neutrally seeded environment would require a different device with higher operational temperatures. The bump at the end of Li target with He in figure 8(c) is due to the lithium supply running out at the surface.
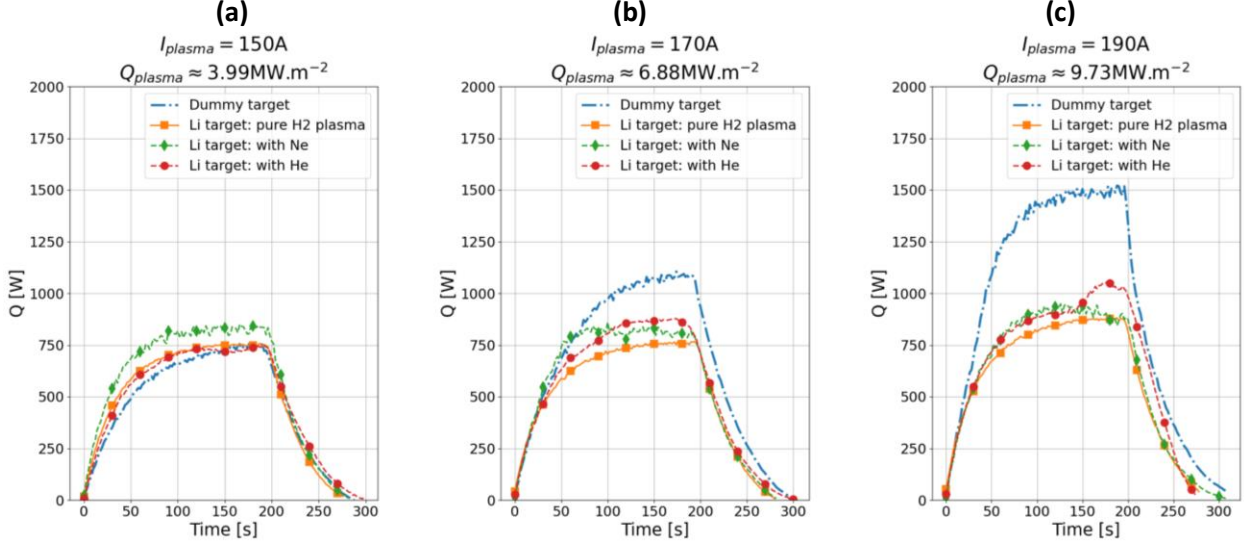
Figure 8: Heat flux measurements of plasmas on the surface of MAGNUM-PSI. four separate experiments are done for each value of heat flux, the first (blue) is a non-lithium plasma, the second (orange) is lithium with just hydrogen, the third (green) is Li with Ne and finally (red) Li with He. (a) 3.99 MWm^{-2}, (b) 6.88 MWm^{-2} and (c) 9.73 MWm^{-2}. It is clear to see that below a threshold of heat flux there is no effect but above some value of heat flux what is seen by the surface is reduces and limited to about 5.5 MWm^{-2}.

III.B. Zapdos-CRANE Modeling

To understand how LVS influences the design of a working LM divertor a knowledge of the conditions that create the vapor shielding is needed. Design and modeling of the behavior of lithium in a future plant, like FNSF, will need to be done using tools like SOLPS-ITER and these need input parameters for how lithium will behave under plasma interactions. The contributing factors to LVS is that as the plasma heat flux interacts with the surface, the surface temperature will increase, and lithium will start to evaporate. At some point the heat flux will reduce until it saturates at some equilibrium, thus locking into the observed temperature and heat flux. There are two factors that contribute to the heat dissipation. The first is the lithium evaporative heat flux and heat lost to lithium sputtering. The second is the lithium vapor cloud itself radiating power away from the target via plasma chemistry.

These parameters are determined by a 1D model that uses a plasma chemistry code (CRANE) and is couples to a plasma transport solver (ZAPDOS). The evaporative lithium particle flux J_{Li} can be modeled from past data and existing empirical relations **[34-36]** as:

$$J_{Li}(T_{surf}) = e^{-T_{surf}} + A\left[1 - \frac{1}{1 + e^{\left(\frac{T_{surf}-c}{s}\right)}}\right],$$

with T_{surf} the lithium surface temperature and A, c and s are fitting parameters. The evaporative heat flux Q_{Li}^{vap} is obtained from J_{Li}, the lithium heat of vaporization h_{Li} and Avogadro's number N_A as:

$$Q_{Li}^{vap} = \frac{h_{Li} \times J_{Li}}{N_A}.$$

To determine the total heat dissipation, also accounting for the plasma chemistry, a heat diffusion model is solved correcting for the heat flux by ΔQ such that an observed locking temperature is observed. This gives:

$$\Delta Q(T_{surf}) = BT_{surf} + C\left[1 + erf\left(\frac{T_{surf} - \mu}{\sigma_m}\right)\right] + D,$$

with B, C, D, μ and σ_m being fitting parameters. Using as a reference one of the intermediate-power shots from the Magnum-PSI campaign where the heat flux is 6 MW.m^{-2} on the solid target and 4.5 MW.m^{-2} on the lithium target, some numerical values can be obtained. The dissipated heat by lithium for this shot is of 1.5 MW.m^{-2} or 265 W, knowing the area of the used targets. The lithium surface temperature at this power setting was measured via an infrared camera to be 650 °C. This gives a maximum evaporative heat flux of $Q_{Li}^{vap} = 45$ W, assuming no redeposition. We can assume that at the temperatures of Magnum-PSI, losses via sputtering are low, and lithium evaporation and sputtering combine to dissipate the 45 W computed with the zero redeposition assumption. This leaves a total of $Q_{Li}^{chem} = 220$ W at least to be dissipated via plasma chemistry.

Hence, excitation and ionization of lithium atoms are probably the most likely mechanisms for the energy dissipation. These are driven by electron collisions. The rate coefficients can be obtained by integrating the reactions cross-sections over a Maxwellian distribution:

$$k = \int_E \sigma(E)\sqrt{\frac{2E}{\mu_m}}y(E)dE,$$

with σ the cross-section, μ_m is the reduced mass and $y(E)$ the Maxwellian distribution. The measured electron temperatures during the Magnum-PSI shots of interest here using Thomson scattering were about 1.2 eV. The power loss per lithium atom can then be found for a particular reaction as:

$$P_{loss} = kn_e\Delta E.$$

This leads to the values shown in table 1 for few excitation ionization reactions. The power losses per lithium atom displayed in table 1 suggest that the power dissipation is achieved mainly through the excitation of the ground state lithium atoms and the ionization of excited lithium atoms. However, the de-excitation reaction rates are much higher than the excitation rates for the experimental plasma parameters proper to the studied shots, as shown in figure 9. Hence, only excitation of the ground state lithium atoms

Excitation power loss		Ionization power loss	
Reaction	P_{loss} [MeV/s]	Reaction	P_{loss} [MeV/s]
$e + Li(2s) \rightarrow e + Li(2p)$	73.6914	$e + Li(2s) \rightarrow Li^+ + 2e$	0.7229
$e + Li(2s) \rightarrow e + Li(3s)$	4.4306	$e + Li(2p) \rightarrow Li^+ + 2e$	7.8615
$e + Li(2s) \rightarrow e + Li(3p)$	2.1462	$e + Li(3s) \rightarrow Li^+ + 2e$	56.4405
$e + Li(2s) \rightarrow e + Li(3d)$	2.9590	$e + Li(3p) \rightarrow Li^+ + 2e$	111.1002
		$e + Li(2d) \rightarrow Li^+ + 2e$	118.9097

Table 1: Excitation and Ionization power losses for different Li species.

is significant at power radiation inside the vapor cloud. As soon as a lithium atom gets excited, it is much more likely to de-excite instantly than to ionize.
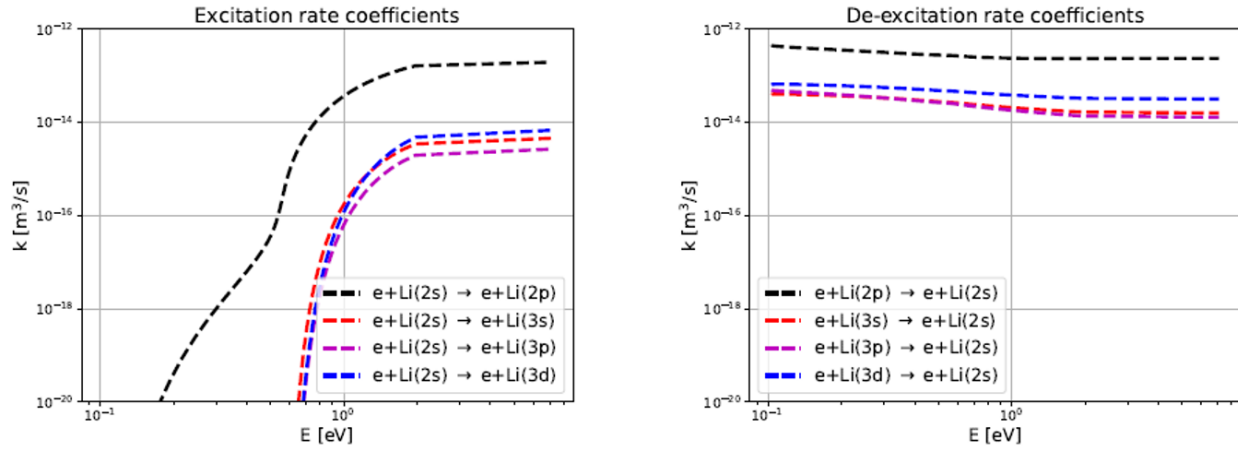

Figure 9: (a) Excitation and (b) de-excitation rates for lithium species. This shows that the de-excitation reaction rates are much higher than the excitation ones.
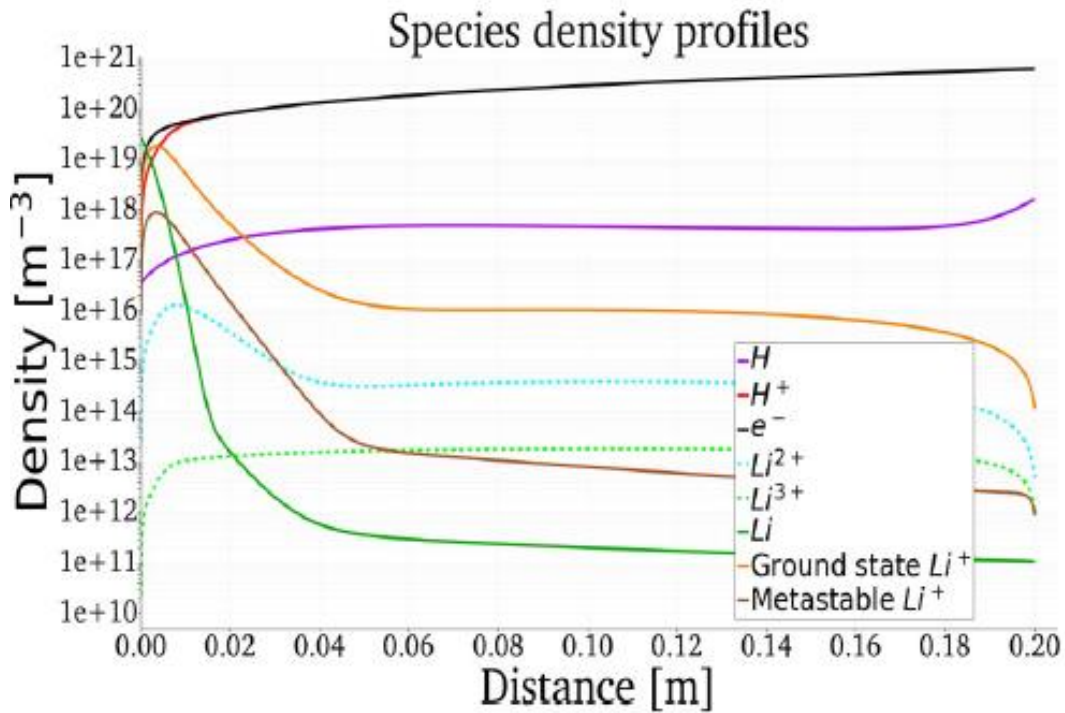

Figure 10: Density profiles for different species within the vapor cloud. This not only includes the lithium species but also incoming plasma

A more thorough analysis can be carried out via the use of Zapdos-CRANE. CRANE allows for a very rich reaction network to be implemented with no limit to the number of reactions which can be traced, while Zapdos can track the transport of the different species and give back spatial profiles for the species concentrations or plasma parameters. An initial model implementation in Zapdos-CRANE gave back the species density profiles shown in figure 10. Experimental benchmarks from the Magnum-PSI experimental

campaigns have been obtained and are being implemented into the Zapdos-CRANE model to properly capture the formation of the vapor cloud and determine the different power dissipation mechanisms.

IV. Note on Helium Retention

The third goal of the program was to start looking at hydrogen and helium retention. Experiments performed in helium plasmas using lithium were performed on the Hybrid Illinois Device for Research and Applications (HIDRA) [37,38]. These experiments were not directly associated with the LMPFC program but have direct consequences for the program. Liquid lithium was introduced into the plasma using the material analysis test-stand [39] and a lithium injector [40]. The aim of the experiments was to test porous tungsten samples in helium plasma without and with lithium. The effect of the lithium on the performance of the plasma and reduction in recycling inside HIDRA showed that there is a more interesting phenomenon to be explored. The results are described in Andruczyk et al. [41] The fact that lithium pumped helium is of utmost importance and is one of the main goals of the LMPFC program set out. HIDRA is considered to have impurities mainly through water vapor and hydrogen and oxygen is seen spectroscopically as well as on RGA's. However, when lithium is present the levels of these also drop significantly. Thus, this suggests that hydrogen and helium can indeed be pumped by lithium. This is an extremely important result for future liquid metal PFC designs for future devices.

V. Future experiments

Though much headway has been made in the understanding of lithium in a vacuum system and its operation with a loop, the ability to wet a surface fully still needs to be achieved and under different conditions such as the angle of the surface and flow velocity. The material that the PFC surface will be made from is also important. Not only does it need to operate with lithium, but it also needs to be able to hold up to the corrosiveness of lithium. Future experiments will have a lithium loop where different samples can be inserted into the loop. The loop is shown in figure 11. The exposure will need to be done for hundreds of hours and the mass reduction in the samples will determine the corrosion rate. Using surface analysis facilities at UIUC will also be able to determine the surface changes that occur.

Lithium vapor shielding needs to be demonstrated in a toroidal environment. The steady-state operation of HIDRA provides a platform for this to happen. Surfaces mounted in HIDRA-MAT can be exposed to plasmas for up to 5400 s. The surface temperature is monitored and thus if a locking temperature is observed will be an indication of the LVS being established.

Understanding the exact mechanism for why lithium pumps helium will be important as well. It is clear that helium is pumped by lithium, but the actual mechanism is not yet understood and if that will translate to a flowing system. Pasts experiments on the FLiER device [42-44] suggest that helium can be pumped by a flowing lithium system. Helium ions were fired into a differentially separated system. The lithium formed the seal between the two chambers and RGA's were used to measure the helium. When the helium was fired into the lithium, it appeared in the second chamber. When switched off, the helium signal disappeared. This with the HIDRA results suggests that helium pumping should be possible. Hydrogen pumping is also important and the ability for lithium to remove hydrogen and then be able to remove it is crucial. Fuel like tritium and deuterium that are not sued in the fusion experiment and are removed with the lithium will need to be extracted and re-used. The rate that this happens needs to be equal or greater than what is absorbed. This will be part of future experiments to determine the absorption rate and the extraction rate [45,46].
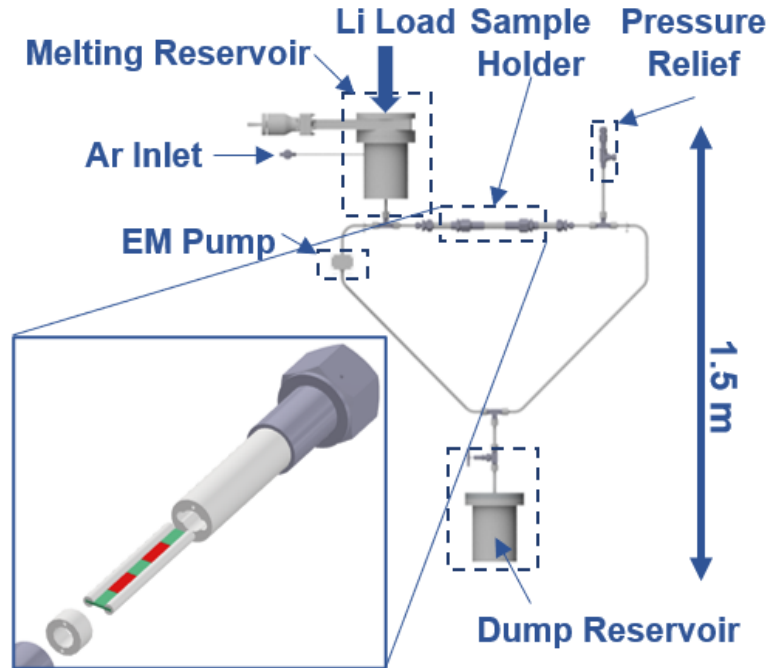
Figure 11: The proposed corrosion loop to test different materials under flowing lithium conditions. This will be done in an argon atmosphere for simplicity.

VI. Summary and Conclusions

The domestic liquid metal PFC program is charged with developing a flowing liquid lithium divertor for a future FNSF or CPP design. UIUC is tasked with developing the loop and surface technology. A flowing liquid lithium loop is now in operation with 1 m/s flow velocities. Marginal wetting of a full plate surface has been achieved and needs to be further developed. One way to do this is to improve the distribution system. Materials compatibility will also be important and a future flowing loop for corrosion studies will be built. An understanding of the lithium vapor cloud is being developed. Lithium vapor shielding is potentially an important effect that needs to be understood as it could be a way to dissipate incoming heat flux to the divertor surface. This is being modeled with Zapdos-CRANE and has been observed in a series of Magnum-PSI experimental campaigns. Future experiments will see LVS experiments in HIDRA under actual toroidal conditions. This will determine the parameters needed to input into SOLPS-ITER to help with the modeling and design of the divertor. Furthermore, future experiments looking at helium and hydrogen retention and recovery will be undertaken.

References

[1] C.E. Kessel et al., Fusion Sci. Technol. **75**, 886 (2019)
[2] G.F. Matthews et al., Phys. Scr. **T138**, 014001 (2009)
[3] H. Zohm et al., Nucl. Fusion **53**, 073019 (2013)
[4] M.J. Baldwin et al., Nucl. Fusion **48**, 035001 (2008)
[5] M.J. Baldwin et al., J. Nucl. Mater. **390-391**, 886 (2009)
[6] M. Ono et al., Fusion Eng. Design **89**, 2838 (2014)
[7] C.E. Kessel et al., Fusion Eng. Design. **135**, 236 (2018)
[8] A. de Castro et al., Phys. Plasmas **28**, 050901 (2021)
[9] D. Mansfield et al., Phys. Plasmas **3**, 1892 (1996)
[10] H.W. Kugel et al., Phys. Plasmas **15**, 056118 (2008)
[11] G.Z. Zuo et al., Plasma Sci. Technol. **12**, 646 (2010)
[12] R. Majeski et al., Phys. Rev. Lett. **97**, 075002 (2006)
[13] A. Maan et al., IEEE Trans. Plasma Sci. **48**, 1463 (2020)
[14] D. Andruczyk et al., J. Fusion. Energy **39**, 441 (2020)
[15] D. Andruczyk et al., Phys. Scr. **T171**, 014067 (2020)
[16] G.G. van Eden et al. Phys. Rev. Letter. **116**, 135002 (2016)
[17] P. Rindt et al., Nucl. Fusion **59**, 056003 (2019)
[18] S. Keniley et al., Plasma Source. Sci. Technol. Accepted Manuscript (2022)
[19] M. Nieto, et al., J. Nucl. Mater. **313–316**, 646 (2003)
[20] P. Fiflis et al., Fusion Eng. Design **89**, 2827 (2014)
[21] J.S. Hu et al., Nucl. Mater. Energy **18**, 99 (2019)
[22] G.Z. Zuo et al., Phys. Plasmas **27**, 052506 (2020)
[23] G. Z. Zuo et al., Phys. Scr. **T171**, 014008 (2020)
[24] C.L. Li et al., Plasma Sci. Technol. Accepted Manuscript (2022)
[25] D. O'Dea et al., Nucl. Fusion, Submitted, Under Review (2022)
[26] G.Z. Zuo et al., Rev. Sci. Instrum. **88**, 123506 (2017)
[27] X. C. Meng et al., Fusion Eng. Design **154**, 111537 (2020)
[28] M. Szott, PhD Thesis (2020)
[29] P. Rindt et al., Nucl. Fusion **59**, 056003 (2019)
[30] G. De Temmerman, et al., Fusion Eng. Design **88**, 483(2013)
[31] S. Mirnov, et al., Plasma Phys. Control. Fusion **48**, 821 (2006)
[32] P. Rindt et al., Nucl. Fusion **59**, 054001 (2019)
[33] J. Lore et al., IEEE Trans. Plasma Sci. Accepted Manuscript (2022) **doi: 10.1109/TPS.2022.3166402**
[34] R.F. Mattas, et al., Fus. Eng. Des. **49–50**, 127 (2000)
[35] A. Khodak et al., IEEE Trans. Plasma Sci. **42**(8), 2161 (2014)
[36] A. Khodak et al., Nucl. Mater. Energy, **26**, 100935 (2021).
[37] D. Andruczyk et al., Fusion Sci. Technol. **68**, 497 (2015)
[38] R. Rizkallah et al., IEEE Trans. Plasma Sci. **46**, 2685 (2018)
[39] A. Shone et al., J. Fusion Energy **39**, 438 (2020)
[40] A. Shone et al., Fusion Eng. Design **180**, 113193 (2022)
[41] D. Andruczyk et al., Plasma Phys. Control. Fusion **64**, 085011 (2022)
[42] J. P. Allain et al., *Fusion Eng. Design*, **61-62**, 245 (2002)
[43] M. Nieto et al., *J. Nucl. Mater.*, **350**, 101 (2006)
[44] R. Stubbers et al., J. Nucl. Mater. **337-339**, 1033 (2005)
[45] M. Christenson et al., Fusion Eng. Design **135**, 81 (2018)
[46] M. Christenson et al., Nucl. Fusion **59**, 026011 (2019)